Photophysical and Theoretical Studies on Luminescent Tetranuclear Coinage Metal Building Blocks

Eduardo J. Fernández,*[,†] Antonio Laguna,*[,‡] José M. López-de-Luzuriaga,[†] Miguel Monge,[†] Manuel Montiel,[†] M. Elena Olmos,[†] and María Rodríguez-Castillo[†]

Departamento de Química, Grupo de Síntesis Química de La Rioja, UA-CSIC, Complejo Científico-Tecnológico, Universidad de La Rioja, 26004-Logroño, Spain, and Instituto de Ciencia de Materiales de Aragón, Departamento de Química Inorgánica, Universidad de Zaragoza-CSIC, 50009-Zaragoza, Spain

Received February 23, 2006

The synthesis, structural characterization, and the study of the photophysical properties of complexes $[Au_2Ag_2(C_6F_5)_4(N{\equiv}CCH_3)_2]_n$ (**1**) and $[Au_2Cu_2(C_6F_5)_4(N{\equiv}CCH_3)_2]_n$ (**2**) have been carried out. The crystal structure of both complexes consists of polymeric chains formed by repetition of Au_2Ag_2 or Au_2Cu_2 units built up by metallophilic Au(I)···M(I) interactions that are linked through Au(I)···Au(I) interactions. Complexes **1** and **2** are brightly luminescent in the solid state at room temperature and at 77 K with lifetimes in the nanosecond range. Both compounds **1** and **2** undergo oligomerization in solution, as observed through UV−vis and excitation spectra in acetonitrile solutions at high concentrations. Thus, a correlation between the excitation spectra in solution at different concentrations and the absorption spectra in the solid state for complex **1** can be established. Time-dependent DFT calculations agree well with the experimental results and support the idea of that the origin of the luminescence of these complexes arises from orbitals located in the tetranuclear Au_2M_2 units.

Introduction

Recent interest in gold(I)−heterometal compounds displaying Au···M (M = closed-shell metal center) interactions was promoted by the interesting features associated with this emerging class of materials such as their theoretical interest,[1] the photophysical properties[2] of the complexes, or their potential applications.[3] Of particular interest are unsupported Au···M interactions, which are not imposed by the ligand architectures. This type of interaction governs the supramolecular arrangements found in the solid state, ranging from discrete molecules to polymeric chains, two-dimensional sheets, or even three-dimensional networks, which are closely related with the rich luminescent properties observed in many cases.[4]

Nevertheless, there is a limited number of closed-shell metal centers that give unsupported interactions with gold(I). The group congeners silver(I) and copper(I) seem to be electronically the most favorable candidates for such Au···M interactions. However, although unsupported Au···Ag interactions are known, they are not a broad family.[5] On the other hand, we have recently reported the first complex displaying unsupported Au(I)···Cu(I) interactions.[6] Therefore, the synthesis of such heterometallic Au−M complexes is a challenge since the systematic comparison among analogous Au−Ag and Au−Cu materials would provide further insight into the theoretical study of the interactions or into the spectroscopic behavior in these classes of complexes. Thus, changes in the heterometal, keeping the rest of the molecule unaltered, would not only provide important spectroscopic information but also serve to prepare new light-emitting polymeric materials suitable for interesting applications such as VOC sensors[3] and LEDs.[7] In addition, the use of Cu(I) as heterometal opens new fields of study since, together with the photophysical properties associated with Au(I), Cu(I) can provide further interesting features such as long emission lifetimes and it can be used as a spectroscopic reporter probe with high affinity for biological substrates.[8]

Polymeric Au−Ag materials such as $[Au_2Ag_2(C_6F_5)_4L_2]_n$ (L = neutral N-, S-, or O-donor ligands)[5a,b] built up through

* To whom correspondence should be addressed. E-mail: eduardo.fernandez@dq.unirioja.es; alaguna@unizar.es.

† Universidad de La Rioja.

‡ Universidad de Zaragoza-CSIC.

(1) a) Pyykkö, P. *Chem. Rev.* **1997**, *97*, 597. (b) Pyykkö, P. *Angew. Chem., Int. Ed.* **2004**, *43*, 4412.

(2) Forward, J. M.; Fackler, J. P., Jr.; Assefa, Z. In *Optoelectronic Properties of Inorganic Compounds*; Roundhill, D. M., Fackler, J. P., Jr., Eds.; Plenum: New York, 1999; pp 195−226.

(3) (a) Fernández, E. J.; Laguna, A.; López-de-Luzuriaga, J. M.; Monge, M. Spanish Patent P200001391, 2003. (b) Fernández, E. J.; López-de-Luzuriaga, J. M.; Monge, M.; Olmos, M. E.; Pérez, J.; Laguna, A.; Mohamed, A. A.; Fackler, J. P., Jr. *J. Am. Chem. Soc.* **2003**, *125*, 2022.

(4) (a) Fernández, E. J.; Laguna, A.; López-de-Luzuriaga, J. M.; Monge, M.; Olmos, M. E.; Pérez, J. *J. Am. Chem. Soc.* **2002**, *124*, 5942. (b) Fernández, E. J.; Laguna, A.; López de Luzuriaga, J. M.; Mendizabal, F.; Monge, M.; Olmos, M. E.; Pérez, J. *Chem. Eur. J.* **2003**, *9*, 456. (c) Fernández, E. J.; Jones, P. G.; Laguna, A.; López-de-Luzuriaga, J. M.; Monge, M.; Olmos, M. E.; Pérez, J. *Inorg. Chem.* **2002**, *41*, 1056. (d) Fernández, E. J.; Laguna, A.; López-de-Luzuriaga, J. M.; Olmos, M. E.; Pérez, J. *Dalton Trans.* **2004**, 1801.

(5) (a) Usón, R.; Laguna, A.; Laguna, M.; Jones, P. G.; Sheldrick, G. M. *Chem. Commun.* **1981**, 1097. (b) Usón, R.; Laguna, A.; Laguna, M.; Manzano, B. R.; Jones, P. G.; Sheldrick, G. M. *J. Chem. Soc., Dalton Trans* **1984**, 285. (c) Usón, R.; Laguna, A.; Laguna, M.; Usón, A.; Jones, P. G.; Erdbrugger, C. F. *Organometallics* **1987**, *6*, 1778. (d) Burini, A.; Fackler, J. P., Jr.; Galassi, R.; Pietroni, B. R.; Staples, R. J. *Chem. Commun.* **1998**, 95. (e) Cerrada, E.; Contel, M.; Valencia, A. D.; Laguna, M.; Gelbrich, T.; Hursthouse, M. B. *Angew. Chem., Int. Ed.* **2000**, *39*, 2353. (f) Burini, A.; Bravi, R.; Fackler, J. P., Jr.; Galassi, R.; Grant, T. A.; Omary, M. A.; Pietroni, B. R.; Staples, R. J. *Inorg. Chem.* **2000**, *39*, 3158. (g) Rawashdeh-Omary, M. A.; Omary, M. A.; Fackler, J. P., Jr. *Inorg. Chim. Acta* **2002**, *334*, 376.

(6) Fernández, E. J.; Laguna, A.; López-de-Luzuriaga, J. M.; Monge, M.; Montiel, M.; Olmos, M. E. *Inorg. Chem.* **2005**, *44*, 1163.

(7) Dias, H. V. R.; Diyabalanage, H. V. K.; Eldabaja, M. G.; Elbjeirami, O.; Rawashdeh-Omary, M. A.; Omary, M. A. *J. Am. Chem. Soc.* **2005**, *127*, 7489.

(8) (a) Ford, P. C.; Cariati, E.; Bourassa, J. *Chem. Rev.* **1999**, *99*, 3625. (b) McMillin, D. R.; McNett, K. M. *Chem. Rev.* **1998**, *98*, 1201.

10.1021/om060181z CCC: $33.50
Publication on Web 06/17/2006

Scheme 1. Synthesis of $[Au_2Ag_2(C_6F_5)_4(N{\equiv}CCH_3)_2]_n$ (1) and $[Au_2Cu_2(C_6F_5)_4(N{\equiv}CCH_3)_2]_n$ (2)

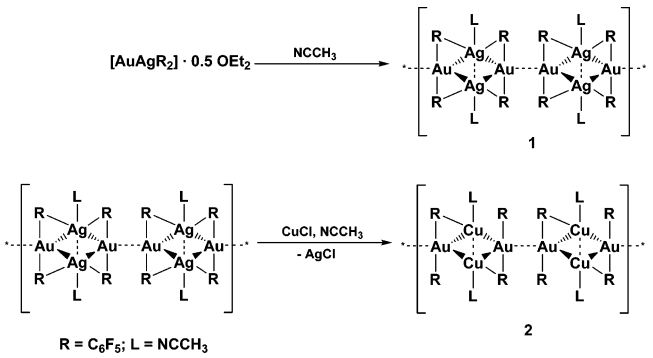

the Lewis acid−base strategy by reaction of $[Au(C_6F_5)_2]^-$ with silver salts are of special interest for several reasons. First, their solid-state structure, consisting of tetranuclear Au_2Ag_2 units linked through unsupported Au(I)···Au(I) interactions, giving extended polymeric chains, also presents additional Au(I)···Ag(I) and Ag(I)···Ag(I) interactions, which makes them very attractive from a photophysical viewpoint. In this sense, this class of materials has been reported to oligomerize in solution mediated by Au(I)···Au(I) interactions upon raising the concentration[9] or act as VOC sensors upon exposure of organic or inorganic vapors to the precursor $[Au_2Ag_2(C_6F_5)_4]_n{\cdot}0.5OEt_2$.[3a] On the other hand, they can act as precursors for the preparation of Au−Cu complexes through a transmetalation reaction with CuCl (see Scheme 1).

Herein we report the synthesis, crystal structures, and photophysical properties of complexes $[Au_2Ag_2(C_6F_5)_4(N{\equiv}CCH_3)_2]_n$ (**1**) and $[Au_2Cu_2(C_6F_5)_4(N{\equiv}CCH_3)_2]_n$ (**2**). To investigate the origin of the luminescence of these analogous complexes, we have also carried out time-dependent DFT calculations that support the experimental assignments.

Results and Discussion

Synthesis and Structural Characterization. Dissolution of the complex $[Au_2Ag_2(C_6F_5)_4]_n{\cdot}0.5OEt_2$ in acetonitrile leads to a colorless solution that upon evaporation to dryness gives rise to complex $[Au_2Ag_2(C_6F_5)_4(N{\equiv}CCH_3)_2]_n$ (**1**) as a bright yellow solid in quantitative yield.

The corresponding gold−copper complex $[Au_2Cu_2(C_6F_5)_4(N{\equiv}CCH_3)_2]_n$ (**2**) was readily synthesized in acetonitrile by reaction of **1** and CuCl (1:1 with respect to silver) in a transmetalation reaction. After filtration of the AgCl formed and evaporation of the solvent to dryness, complex **2** was obtained as an orange solid. Both complexes display similar ^{19}F NMR spectra in which the signals corresponding to the C_6F_5 groups bonded to Au(I) in the $[Au(C_6F_5)_2]^-$ units are observed at −114.59 (F_o), −160.99 (F_p), −162.72 (F_m) ppm and −114.83 (F_o), −161.62 (F_p), −162.82 (F_m) ppm, respectively. All other physical and spectroscopic properties are in accordance with the proposed stoichiometries, and both crystal structures have been established by X-ray diffraction studies.

Crystal Structures. Crystal structures of complexes **1** and **2** were determined by X-ray diffraction from single crystals obtained by slow diffusion of *n*-hexane into a solution of the complex in toluene. Both of them crystallize in the *C*2/*c* space group of the monoclinic system and show very similar cell parameters. Both of them consist of tetranuclear $[Au_2(C_6F_5)_4M_2(N{\equiv}CCH_3)_2]$ (M = Ag (**1**), Cu (**2**)) units (see Figures 1 and 2) linked together via very short aurophilic contacts, resulting in the formation of monodimensional polymers that run parallel to the crystallographic *z* axis (see Supporting Information).

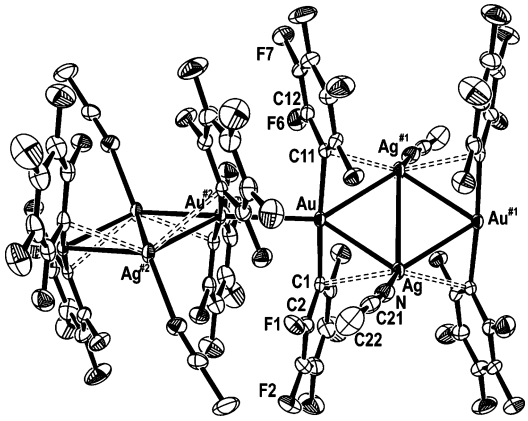

Figure 1. Part of the polymetallic chain of complex **1** with the labeling scheme for the atom positions. Hydrogen atoms have been omitted for clarity.

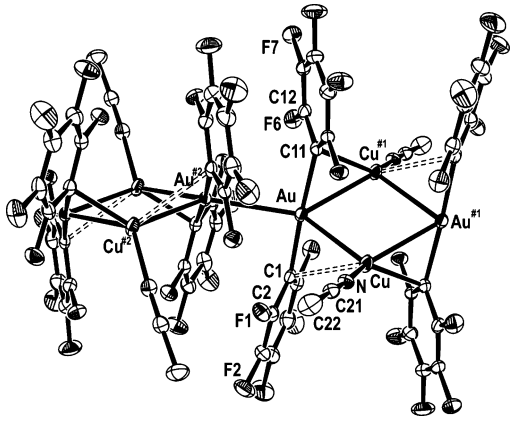

Figure 2. Part of the polymetallic chain of complex **2** with the labeling scheme for the atom positions. Hydrogen atoms have been omitted for clarity.

The molecule lies on a 2-fold symmetry axis, so only half a molecule resides in the asymmetric unit. The intermolecular Au−Au distances of 2.8807(4) Å (**1**) or 2.9129(3) (**2**) Å are shorter than in the related complexes $[Au_2(C_6F_5)_4Ag_2(OMe_2)_2]_n$[9] (3.1674(11) Å) and $[Au_2(C_6F_5)_4Ag_2(C_6H_6)_2]_n$[5c] (3.013(2) Å) and close to that observed in $[Au_2(C_6F_5)_4Ag_2(SC_4H_8)_2]_n$[5a,b] (2.889(2) Å) and suggest a substantial bonding interaction between the gold centers. The gold(I) atoms are linearly coordinated to two pentafluorophenyl groups with additional (and rather uncommon) Au−M bonds within the tetranuclear unit. The Au−Ag bond lengths of 2.7577(5) and 2.7267(5) Å in **1** compare well with those observed in the related complexes $[Au_2(C_6F_5)_4Ag_2L_2]_n$ (L = $OCMe_2$,[9] C_6H_6, or SC_4H_8[5a,b]), while the Au−Cu distances of 2.5741(6) and 2.5876(5) Å in **2** are similar to the Au−Cu distances present in some clusters[10,11] (2.589 and 2.584 Å) and shorter than that found in the polymeric compound $[Cu\{Au(C_6F_5)_2\}(NCMe)(\mu_2\text{-}C_4H_4N_2)]_n$[6] (2.8216(6) Å), which displays unsupported Au−Cu interactions. It is worth mentioning that, taking into account the Au−M distances found in **1**

(9) Fernández, E. J.; Gimeno, M. C.; Laguna, A.; López-de-Luzuriaga, J. M.; Monge, M.; Pyykkö, P.; Sundholm, D. *J. Am. Chem. Soc.* **2000**, *122*, 7287.

(10) Albano, V. G.; Castellari, C.; Femoni, C.; Iapalucci, M. C.; Longoni, G.; Monari, M.; Zacchini S. *J. Cluster Sci.* **2001**, *12*, 75.

(11) Haupt, H.-J.; Seewald, O.; Florke, U.; Buss, V.; Weyhermuller T. *J. Chem. Soc., Dalton Trans.* **2001**, 3329.

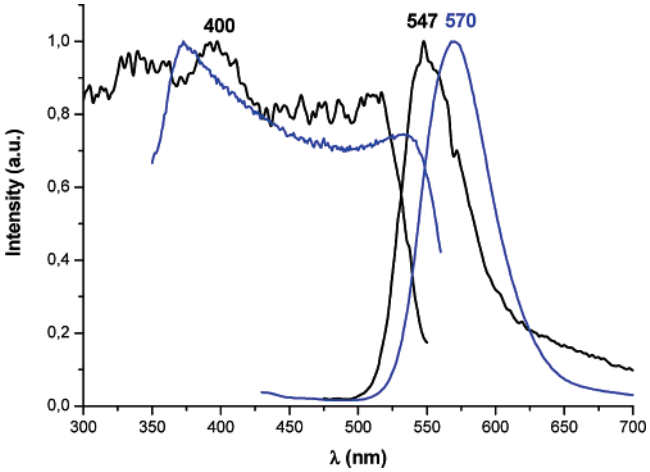

Figure 3. Excitation and emission spectra of **1** (black) and **2** (blue) in the solid state at room temperature.

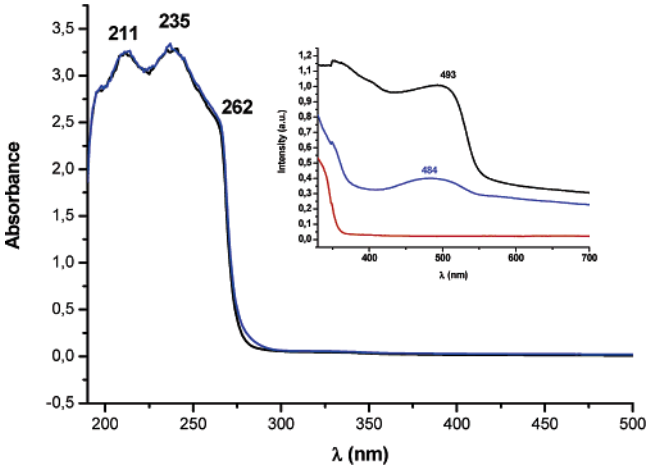

Figure 4. Absorption spectra of **1** (black) and **2** (blue) in 5×10^{-4} M CH_3CN at room temperature. Inset: Absorption spectra of **1** (black), **2** (blue), and $NBu_4[Au(C_6F_5)_2]$ (red) in the solid state.

and **2** and the van der Waals radii for the three metals (Cu: 1.40, Ag: 1.72, Au: 1.66 Å),[12] the Au−M bonding interaction is stronger in the silver derivative **1** than in the copper one **2**. The M^I centers are also bonded to the nitrogen atom of an acetonitrile molecule, showing M−N bond distances of 2.206(6) Å (**1**) and 1.903(4) Å (**2**).

Although both crystal structures are very similar, there are some differences in their bonding scheme. First, while in **1** all the pentafluorophenyl groups bridge the gold and silver atoms asymmetrically (see Figure 1) with Au−C distances of 2.055(6) and 2.088(6) Å and Ag−C distances of 2.508(6) and 2.687(6) Å, in **2** one of the crystallographically independent C_6F_5 groups also acts as an asymmetric bridge between gold and copper with Au−C and Cu−C distances of 2.043(5) and 2.8642(38) Å, respectively, while the second pentafluorophenyl group binds Au and Cu more symmetrically (see Figure 2) with Au−C and Cu−C bond distances of 2.090(4) and 2.141 Å, respectively. The second difference between **1** and **2** is the presence of an additional Ag···Ag contact within the tetranuclear core of 3.1084(10) Å in **1**, which is absent in **2**, where the Cu−Cu separation of 3.0197(11) Å is longer than twice the van der Waals radius of copper (2.80 Å).[12] The Ag−Ag distance in **1** is slightly shorter than in the acetone derivative $[Au_2(C_6F_5)_4Ag_2(OCMe_2)_2]_n$[9] (3.1810(13) Å), which displays a very similar crystal structure.

Photophysical Studies. The two reported complexes display a very intense luminescence in the solid state. These emit at 547 nm (exc. 400; **1**) and 570 nm (exc. 400 nm; **2**) at room temperature, emissions that are shifted to 567 nm (max. exc. 365, 490 nm) or 594 nm (max. exc. 364, 519 nm), respectively, when the temperature is lowered to 77 K. The excitation spectra show very complicated profiles, and the emissions are independent of the excitation wavelengths, with red edge limits of ca. 525 nm (**1**) and 550 nm (**2**).

The lifetime measurements in the solid state at room temperature [$\tau_1 = 231$, $\tau_2 = 84$ ($\chi^2 = 1.5$) for **1**; $\tau_1 = 592$, $\tau_2 = 163$ ns ($\chi^2 = 1.3$) for **2**] within the nanosecond time scale together with the short Stokes' shifts may suggest that the emissions are associated with spin-allowed transitions. Nevertheless, the expected strong spin−orbit coupling in these complexes makes a conclusive assignment difficult. Their absorption spectra in acetonitrile (Figure 4) (5×10^{-4} M) display a similar profile, with bands at 211 ($\epsilon = 6.5 \times 10^3$), 235 ($\epsilon = 6.5 \times 10^3$), and 262 nm ($\epsilon = 5.1 \times 10^3$ mol^{-1} dm^3 cm^{-1}). On the basis of the high energy of the absorptions as well as on the similarity of the spectra registered for **1**, **2**, and the precursor $NBu_4[Au(C_6F_5)_2]$ (which displays bands at 210, 236, and 264 nm with similar intensities), we tentatively assign them to $\pi\pi^*$ transitions in the pentafluorophenyl rings. This assignment has been also described in other polymeric complexes built by acid (metal salts)/basic (bisperhalophenylgold(I)) stacking.[4b,6,9] In contrast, the solid-state absorption spectra display interesting features, because, in addition to a strong and wide absorption band between 250 and ca. 350 nm, an absorption at lower energies appears. In complex **1** that band is placed at 493 nm and in **2** at 484 nm. The profile of these absorption spectra in the solid state resembles those of the excitation spectra, indicating that these absorptions give rise to the observed emissions. On the other hand, the corresponding absorption spectrum of the precursor $NBu_4[Au(C_6F_5)_2]$ salt in the solid state does not display any absorption at similar values. This result is indicative of transitions influenced by the gold−gold or gold−heterometal (Au−Ag or Au−Cu) interactions, since the precursor gold complex does not display any band at similar energies.

Interestingly, in acetonitrile solutions, an increase of the initial concentrations leads to a gradual red shift in the absorption edges of the more intense bands for both complexes, although in the case of complex **1** this is more pronounced for similar concentration values. For instance, an increase from 5×10^{-4} M to 2.5×10^{-2} M shifts the band edge by about 5000 cm^{-1} for the gold−silver complex and by 3800 cm^{-1} in the case of the gold−copper one.

These results are interpreted in terms of molecular aggregation when the concentration increases. In addition, when the concentration is raised, a new, weak shoulder at ca. 325 nm appears in the absorption spectra also for both complexes, whose intensity is concentration dependent and that could be due to an increase in the number of gold−gold interactions between the units that form the oligomers in solution. Concentration near saturation does not give rise to the presence of new bands in the low-energy region. Similar energy values and intensities have been attributed to Au···Au singlet−triplet ($5d\sigma^* \rightarrow 6p_z$) transitions, while the allowed singlet counterpart has been reported at higher energies (ca. 270 nm),[13] and in our case it is probably masked by the absorptions due to the pentafluorophenyl rings and Au−Cu or Au−Ag allowed transitions that appear at similar

(12) http://www.webelements.com.

(13) Fu, W.-F.; Chan, K.-C.; Cheung, K.-K.; Che, C.-M. *Chem. Eur. J.* **2001**, *7*, 4656.

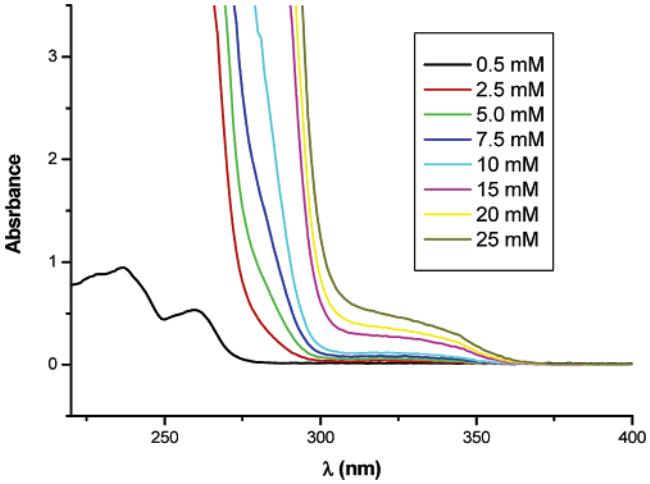

Figure 5. Absorption spectra of **1** in CH_3CN at different concentrations.

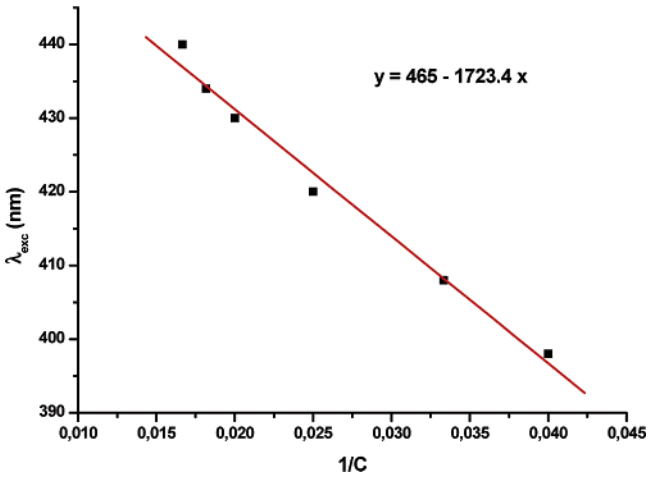

Figure 6. Representation of the inverse of the concentration ($1/C$) vs the excitation wavelength (λ_{exc} (nm)) for complex **1**. The calculated intercept at 465 ± 2.8 nm resembles the maximum of the absorption spectrum in the solid state.

energies. These results are consistent with the extended chain structures for both solids, and in fact, similar spectral changes have also been previously reported in other gold−silver complexes.[5g,9] Nevertheless, from our knowledge this is the first report of a gold−copper complex showing a deviation of the Beer−Lambert law.

The absorption band and the lower excitation energy for the solid is lower than the absorption energies of the concentrated solutions. This result is probably due to the expected lower band gap energy in the extended chain species in the solid state, as opposed to the situation in oligomers of a few units in solution. The absence of well-defined absorption bands in the low-energy regions for the concentrated solutions precludes accurate calculations for the formation constants of oligomers of each compound. Nevertheless, in view of the similar profiles observed for the solid-state absorption bands and those of the excitation spectra, the study of the excitation spectra at these concentrations, whose profiles are well defined, leads to a linear fit (see Figure 6) in which the intercept roughly resembles that observed in the absorption spectrum in the solid state (infinite concentration). This type of behavior has already been reported in the study of absorption[14] or emission[9] spectra.

Although complexes **1** and **2** show the commented similarities, both display different luminescence in solution as a function

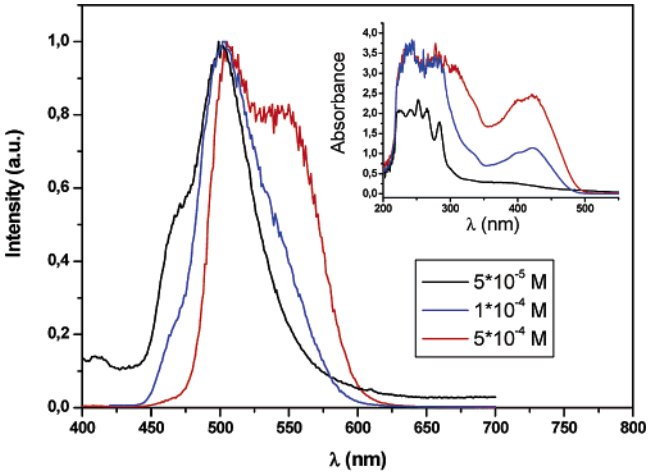

Figure 7. Emission spectra of complex **1** in 5×10^{-5} M (black), 10^{-4} M (blue), and 5×10^{-4} M (red) glassy solution at 77 K. The inset displays the absorption spectra of complex **1** in 5×10^{-5} M (black), 10^{-4} M (blue), and 5×10^{-4} M (red) EtOH/MeOH/CH_2Cl_2 glass solution at 77 K.

of the concentration, the temperature, or the solvent employed. Thus, degassed acetonitrile solutions (ca. 5×10^{-4} M) of complexes **1** and **2** become colorless and nonluminescent. Evaporation of the solvent regenerates the color and the initial optical properties without apparent degradation of the products, even after several solution/evaporation cycles. Nevertheless, interesting results are obtained when both complexes are measured in glass media (EtOH/MeOH/CH_2Cl_2, v/v/v, 8:2:1) at 77 K at different concentrations. The absorption spectrum of complex **1** at low concentration (5×10^{-5} M) shows high-energy bands assigned to intraligand transitions (IL) and a much weaker absorption placed at around 425 nm. The latter is concentration dependent, showing a red-shift of the band edge as the concentration increases, with a better defined profile showing the presence of shoulders at lower energies (see inset in Figure 7). Complex **1** also shows up to three concentration-dependent emission bands (excitations at the low-energy absorptions) when the concentration is raised from 5×10^{-5} M to 5×10^{-4} M (Figure 7). Thus, at the lowest concentration (5×10^{-5} M, black line) complex **1** displays a strong emission band at 501 nm with a shoulder placed at higher energy (470 nm); at intermediate concentration (10^{-4} M, blue line) the higher energy band at 470 nm diminishes its intensity and, in addition to the main band at 501 nm, a new shoulder appears at ca. 540 nm, which is completely defined at the highest concentration (5×10^{-4} M, red line). These results seem to be in accordance with the simultaneous presence of oligomers of different length in solution as a function of the concentration. Therefore, at high concentrations the oligomers of larger sizes are predominant and, consequently, the emission appears red-shifted, in agreement with the behavior observed in the absorption and excitation spectra in solution at different concentrations and at different temperatures.

The lack of any emission for the gold−copper complex in these donor solvents can be interpreted in terms of a quenching effect by coordination of donor-solvent molecules to the copper centers. That exciplex quenching mechanism could be related to an associative attack by the solvent, which produces the stabilization of the excited state and destabilization of the ground

(14) (a) Tang, S. S.; Chang, C.-P.; Lin, I. J. B.; Liou, L.-S.; Wang, J.-C. *Inorg. Chem.* **1997**, *36*, 2294. (b) Rawashdeh-Omary, M. A.; Omary, M. A.; Patterson, H. H. *J. Am. Chem. Soc.* **2000**, *122*, 10371.

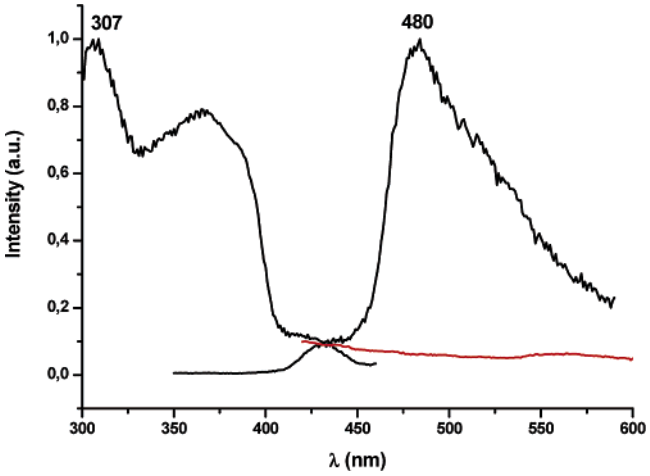

Figure 8. Excitation and emission spectra of complex **2** in toluene at 77 K (black) and emission quenching in acetonitrile at 77 K (red).

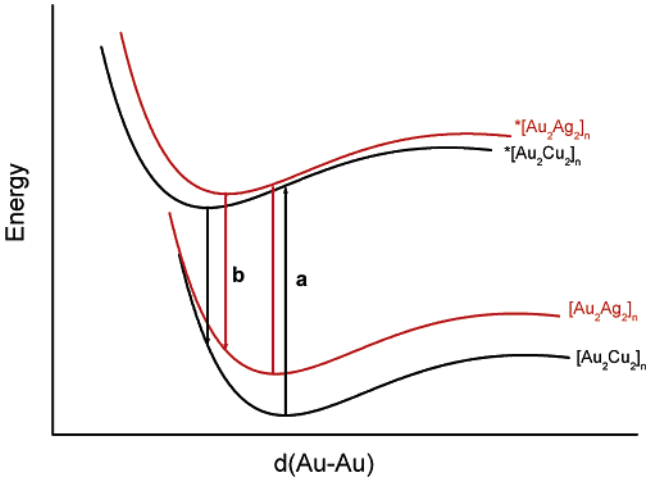

Figure 9. Proposed photophysical model for the $[Au_2M_2R_4L_2]_n$ (M = Ag, Cu) complexes: (a) solid-state absorption bands; (b) solid-state emission bands.

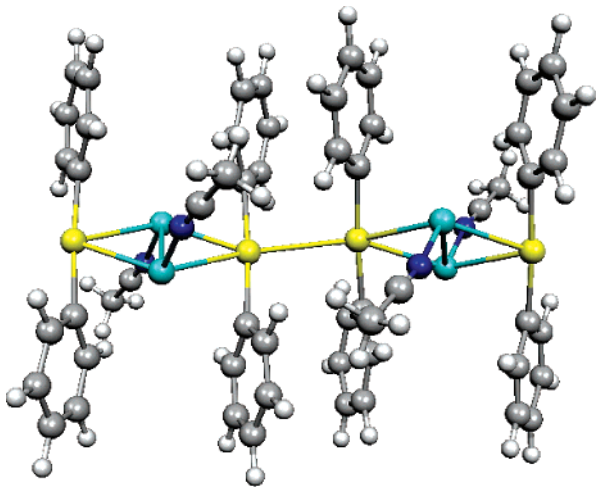

Figure 10. Theoretical model system $[Au_2Ag_2(C_6H_5)_4(N{\equiv}CCH_3)_2]_2$, **1a**.

state, which inevitably promotes quenching.[8b,15] In this sense, McMillin et al. have reported that in donor solvents the possibility of expanding the coordination number renders the copper(I) systems to an unusual, but very effective form of exciplex quenching.[15j] By contrast, in the case of dichlorometane or toluene, their lesser coordinative abilities prevent the formation of the exciplexes, and thus, measurements in these solvents at 77 K give values of 514 (exc. 350) or 481 nm (exc. 365 nm) for this complex.

Finally, the fact that the gold−copper complex displays a lesser energetic emission in the solid state compared to the gold−silver compound is in accordance with the data obtained for other copper and silver complexes bonded to electron-rich donating groups[16] and could be justified by the slightly easier possibility of reduction of Cu(I) compared to Ag(I).[17] Nevertheless, as is observed in the theoretical calculations section, the copper or silver centers are also contributors to the orbital origin of the transitions. In this sense, the lower energy emission in the Cu complex is more likely associated with the influence of copper and silver on the Au···Au interactions. Consequently, a transition located in the tetranuclear core whose energy is influenced by molecular aggregation could also be a plausible assignation in these complexes (Figure 9).

Time-Dependent DFT Calculations. In view of the results reported in the photophysical studies section, single-point DFT and time-dependent DFT calculations have been carried out on model systems $[Au_2Ag_2(C_6H_5)_4(N{\equiv}CCH_3)_2]_2$ (**1a**) and $[Au_2Cu_2(C_6H_5)_4(N{\equiv}CCH_3)_2]_2$ (**2a**). These theoretical models represent an approximation of compounds **1** and **2** in the solid state since all the interactions responsible for the polymeric arrangements are considered in the model systems. Thus, both models display a C_2 symmetry and have been built up from the X-ray diffraction results.We have analyzed first the electronic structure of models **1a** and **2a** obtained through single-point DFT calculations. Thus, we can check the contribution of each part of the molecules to the frontier orbitals. In the case of the occupied orbitals we can perform a population analysis from which we observe that from HOMO−1 to HOMO−16 the orbitals are mainly centered on the ligands with some contribution from the metal centers. Nevertheless, the population analysis shows that the HOMO orbital is mainly centered on the gold atoms that maintain an interaction, and the analysis of the shape of this orbital reveals an $nd_{z^2}\sigma^*$ character. On the other hand, the lowest unoccupied orbitals cannot be analyzed by a population analysis, but we can check the shape of the orbitals on models **1a** and **2a**. The LUMO orbital for both model systems displays bonding electronic density between the two gold atoms and the two silver atoms (or copper) that are in close proximity, which would correspond mostly to an np character.Thus, in view of the electronic structure calculations of models **1a** and **2a** we can derive that the presence of the different intermetallic interactions plays a significant role in the frontier orbitals. This theoretical result is in accordance with the experimental photophysical observations. Thus, for instance, the absence of luminescence in solution at room temperature agrees with the rupture of gold−gold interactions. In contrast, the oligomerization process in solution at high concentrations is also in accordance with the formation of $[Au_2M_2]_n$ oligomers in which intermetallic interactions appear even in solution, giving rise to luminescence. Moreover, the emission in the solid state can

(15) (a) Sakaki, S.; Mizutani, H.; Kase, Y. *Inorg. Chem.* **1992**, *31*, 4575. (b) Eggleston, M. K.; McMillin, D. R.; Koenig, K. S.; Pallenberg, J. A. *Inorg. Chem.* **1997**, *36*, 172. (c) Everly, R. M.; Ziesel, R.; Suffert, J.; McMillin, D. R. *Inorg. Chem.* **1991**, *30*, 559. (d) Shinozaki, K.; Kaizu, Y. *Bull. Chem. Soc. Jpn.*, **1994**, *67*, 2435. (e) Armaroli, N. *Chem. Soc. Rev.* **2001**, *30*, 113. (f) Ford, P. C.; Cariati, E.; Bourassa, J. *Chem. Rev.* **1999**, *99*, 3625. (g) McMillin, D. R.; Kirchoff, J. R.; Goodwin, K. V. *Coord. Chem. Rev.* **1985**, *64*, 83. (h) Stacy, E. M.; McMillin, D. R. *Inorg. Chem.* **1990**, *29*, 393. (i) Horváth, A.; Stevenson, K. L. *Coord. Chem. Rev.* **1996**, *153*, 57. (j) Cuttell, D. G.; Kuang, S.-M.; Fanwick, P. E.; McMillin, D. R.; Walton, R. A. *J. Am. Chem. Soc.* **2002**, *124*, 6.

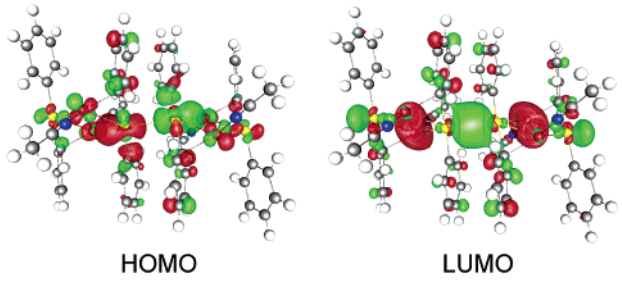

Figure 11. HOMO and LUMO orbitals for model system $[Au_2Cu_2(C_6H_5)_4(N{\equiv}CCH_3)_2]_2$, **2a**.

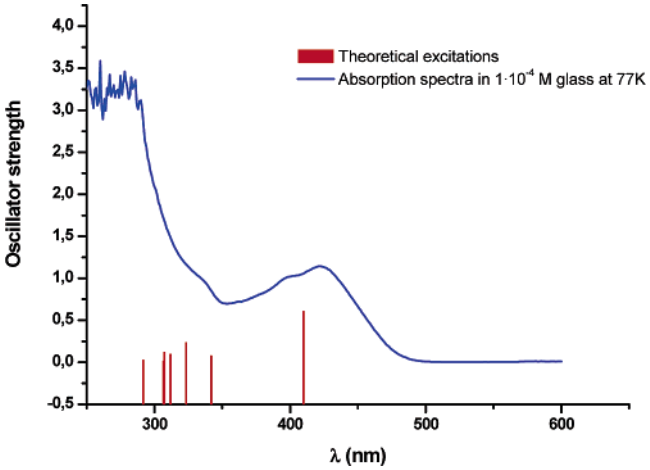

Figure 12. Experimental excitation spectra of complex **1** in the solid state at room temperature (black) and theoretical excitations (red) for model system $[Au_2Ag_2(C_6H_5)_4(N{\equiv}CCH_3)_2]_2$, **1a**.

also be attributed to the presence of metallophilic interactions in the extended polymeric structures in view of the character of the frontier orbitals, probably involved in the excitations responsible for the luminescent behavior.

The above theoretical assignments were confirmed by TD-DFT calculations of the first few allowed singlet excitations on models **1a** and **2a**. Since we currently cannot estimate the contribution of spin−orbit effects to the triplet transitions and the experimental data that are in the nanosecond range, indicating fluorescence, only singlet−singlet transitions were considered in these quasirelativistic calculations. By checking Laporte's rule we observe that for the point group C_2 the HOMO−LUMO transition is dipole-allowed.

In Figure 12 we compare the most intense theoretical excitations with the experimental excitation spectrum of complex **1** in glass media at 77 K (see Supporting Information for complex **2**). In both cases the predicted energy values for the excitations show that the theoretical profiles appear at slightly higher energy than those obtained experimentally. Nevertheless, we can separate both the experimental and the predicted spectra into two energetic regions: one corresponding to the theoretical HOMO−LUMO transition and the other corresponding to higher energy excitations. Another interesting aspect of the predicted excitations is the large oscillator strength obtained for the HOMO−LUMO transition for both models compared to the rest of the excitations.

The analysis of the HOMO−LUMO transitions shows that the most important orbitals involved in the transitions are 142b (HOMO) and 143a (LUMO) in the case of model **1a** and 152b (HOMO) and 153a (LUMO) in the case of model **2a**. These predicted transitions at 410 nm for the Au−Ag model and 395 nm for the Au−Cu model can be assigned to the experimental absorption in the solid state at 493 and 484 nm for complex **1** and **2**, respectively. Moreover, the character of the orbitals involved in these HOMO−LUMO transitions agrees with the experimentally proposed photophysical model in which a transition from an antibonding occupied orbital mainly centered in the gold interacting atoms with contribution from the heterometals to a bonding virtual orbital located between Au and Ag (or Cu) centers would be responsible for the luminescent behavior. Consequently, we propose that the emission would arise from a transition located in the tetranuclear units.

Experimental Section

General Procedures. The compound $[AuAg(C_6F_5)_2]{\cdot}0.5OEt_2$ was prepared by literature methods.[3a] Solvents (spectroscopic grade) used in the spectroscopic studies were degassed prior to use.

Instrumentation. Infrared spectra were recorded in the 4000−200 cm^{-1} range on a Perkin-Elmer FT-IR Spectrum 1000 spectrophotometer, using Nujol mulls between polyethylene sheets. C, H, N, and S analyses were carried out with a C.E. Instrument EA-1110 CHNS-O microanalyzer. Mass spectra were recorded on a HP-5989B API-electrospray mass spectrometer with interface 59987A. ^1H, ^{19}F, and $^{31}P\{^1H\}$ NMR spectra were recorded on a Bruker Avance 400 in $N{\equiv}CCD_3$ solutions. Chemical shifts are quoted relative to $SiMe_4$ (^1H external), $CFCl_3$ (^{19}F external), and H_3PO_4 (85%) (^{31}P, external). Absorption spectra in solution were registered on a Hewlett-Packard 8453 diode array UV−visible spectrophotometer. Absorption spectra in the solid state were obtained on a Cary-500 UV−vis−NIR spectrophotometer equipped with a praying mantis diffuse reflectance accessory. Excitation and emission spectra as well as lifetime measurements were recorded with a Jobin-Yvon Horiba Fluorolog 3-22 Tau-3 spectrofluorimeter.

Synthesis of $[Au_2Ag_2(C_6F_5)_4(N{\equiv}CCH_3)_2]_n$, 1. The orange solid $[AuAg(C_6F_5)_2]{\cdot}1/2Et_2O$ (0.090 g, 0.141 mmol) in 15 mL of acetonitrile was stirred for 30 min at room temperature. Evaporation of the solvent under vacuum gave rise to a yellow-green solid in almost quantitative yield. Mass spectrum (ES−): *m/z* 1170 ($[Au_2Ag(C_6F_5)_2]^-$). Anal. (%) Calcd for $C_{28}H_6Ag_2Au_2F_{20}N_2$: C, 24.73; H, 0.44; N, 2.06. Found: C, 24.55; H, 0.40; N, 2.05. ^{19}F NMR (282 MHz, $N{\equiv}CCD_3$): δ −114.59 (m, 4F, F_o), −160.99 (t, 2F, F_p, $^3J(F_p{-}F_m) = 19.3$ Hz), −162.72 (m, 4F, F_m). ^1H NMR (400 MHz, $N{\equiv}CCD_3$): δ 1.95 (s, 3H, CH_3). FT-IR (Nujol mulls): ν 2315, 2288 cm^{-1} (C≡N), ν 1506, 967, 783 cm^{-1} (Au−C_6F_5).

Synthesis of $[Au_2Cu_2(C_6F_5)_4(N{\equiv}CCH_3)_2]_n$, 2. To a solution of $[Au_2Ag_2(C_6F_5)_4(N{\equiv}CCH_3)_2]_n$ (0.096 g, 0.141 mmol) in acetonitrile (15 mL) was added CuCl (0.014 g, 0.141 mmol), and a white precipitate (AgCl) was immediately formed. The reaction mixture was stirred for 2 h, filtered, and evaporated to dryness under vacuum. Upon removal of the solvent, an orange solid was obtained (yield 67%). Mass spectrum (ES−): *m/z* 1125 ($[Au_2Cu(C_6F_5)_4]^-$). Anal. (%) Calcd for $C_{28}H_6Au_2Cu_2F_{20}N_2$: C, 26.45; H, 0.47; N, 2.20. Found: C, 26.30; H, 0.39; N, 2.12. ^{19}F NMR (282 MHz, $N{\equiv}CCD_3$): δ −114.83 (m, 4F, F_o), −161.62 (t, 2F, F_p, $^3J(F_p{-}F_m) = 19.4$ Hz), −162.82 (m, 4F, F_m). ^1H NMR (400 MHz, $N{\equiv}CCD_3$): δ 1.95 (s, 3H, CH_3). FT-IR (Nujol mulls): ν 2328, 2297 cm^{-1} (C≡N), ν 1498, 957, 781 cm^{-1} (Au−C_6F_5).

Crystallography. The crystals were mounted in inert oil on glass fibers and transferred to the cold gas stream of a Nonius Kappa CCD diffractometer equipped with an Oxford Instruments low-temperature attachment. Data were collected by monochromated Mo Kα radiation ($\lambda = 0.71073$ Å). Scan type: ω and ϕ. Absorption corrections: numerical (based on multiple scans). The structures were solved by direct methods and refined on F^2 using the program SHELXL-97.[18] All non-hydrogen atoms were anisotropically

(16) Yam, V. W. W.; Lo, K. K. W.; Fung, W. K. M.; Wang, C. R. *Coord. Chem. Rev.* **1998**, *171*, 17.

Table 1. Data Collection and Structure Refinement Details for Complexes 1 and 2

	1	**2**
chemical formula	$C_{28}H_6Ag_2Au_2F_{20}N_2$	$C_{28}H_6Au_2Cu_2F_{20}N_2$
cryst habit	orange prism	orange prism
cryst size/ mm	0.10 × 0.10 × 0.06	0.15 × 0.05 × 0.05
cryst syst	monoclinic	monoclinic
space group	*C*2/*c*	*C*2/*c*
a/Å	14.3431(3)	14.0107(2)
b/Å	16.5223(4)	16.4487(4)
c/Å	14.6397(3)	14.0295(3)
β/deg	111.655(1)	106.119(1)
U/Å^3	3224.47(12)	3106.10(11)
Z	4	4
D_c/g cm^{-3}	2.802	2.719
M	1360.02	1271.36
F(000)	2480	2336
T/°C	−100	−100
$2\theta_{max}$/deg	56	56
μ(Mo Kα)/mm^{-1}	10.410	10.915
no. of reflns measd	13 078	24 691
no. of unique reflns	3837	3704
R_{int}	0.0510	0.0729
R^a ($I > 2\sigma(I)$)	0.0361	0.0289
wR^b (F^2, all reflns)	0.0781	0.0578
no. of params	245	245
no. of restraints	97	74
S^c	1.033	1.034
max. $\Delta\rho$/e Å^{-3}	2.517	1.435

[a] $R(F) = \sum||F_o| - |F_c||/\sum|F_o|$. [b] $wR(F^2) = [\sum\{w(F_o^2 - F_c^2)^2\}/\sum\{w(F_o^2)^2\}]^{0.5}$; $w^{-1} = \sigma^2(F_o^2) + (aP)^2 + bP$, where $P = [F_o^2 + 2F_c^2]/3$ and *a* and *b* are constants adjusted by the program. [c] $S = [\sum\{w(F_o^2 - F_c^2)^2\}/(n - p)]^{0.5}$, where *n* is the number of data and *p* the number of parameters.

Table 2. Selected Bond Lengths [Å] and Angles [deg] for Complex 1[a]

Au−Au#2	2.8807(4)	Au−C(1)	2.055(6)
Au−Ag	2.7577(5)	Au−C(11)	2.088(6)
Au−Ag#1	2.7267(5)	Ag−N	2.206(6)
Ag−Ag#1	3.1084(10)		
C(1)−Au−C(11)	175.9(2)	C(1)−Au−Ag#1	114.93(14)
C(11)−Au−Ag#1	61.10(15)	C(1)−Au−Ag	66.00(15)
C(11)−Au−Ag	110.73(15)	Ag#1−Au−Ag	69.048(17)
C(1)−Au−Au#2	95.45(14)	C(11)−Au−Au#2	88.63(15)
Ag#1−Au−Au#2	146.964(15)	Ag−Au−Au#2	139.922(11)
N−Ag−C(11)#1	124.8(2)	N−Ag−C(1)	107.7(2)
C(11)#1−Ag−C(1)	114.63(19)	N−Ag−Au#1	116.90(17)
C(11)#1−Ag−Au#1	46.79(14)	C(1)−Ag−Au#1	133.59(11)
N−Ag−Au	101.88(15)	C(11)#1−Ag−Au	133.11(13)
C(1)−Ag−Au	44.34(13)	Au#1−Ag−Au	110.952(17)
N−Ag−Ag#1	125.41(16)	C(11)#1−Ag−Ag#1	90.32(13)
C(1)−Ag−Ag#1	88.30(13)	Au#1−Ag−Ag#1	55.947(15)
Au−Ag−Ag#1	55.006(14)		

[a] Symmetry transformations used to generate equivalent atoms: #1 −*x*, −*y*+1, −*z*; #2 −*x*, *y*, −*z*+1/2.

refined, and hydrogen atoms were included using a riding model. Further details on the data collection and refinement methods can be found in Table 1. Selected bond lengths and angles are shown in Tables 2 and 3, and crystal structures of **1** and **2** can be seen in Figures 1 and 2. CCDC-243690-243691 contains the supplementary crystallographic data for this paper. These data can be obtained free of charge via www.ccdc.cam.ac.uk/conts/retrieving.html (or from the Cambridge Crystallographic Data Centre, 12 Union Road, Cambridge CB2 1EZ, UK; fax: (+44) 1223-336-033; or e-mail: deposit@ccdc.cam.ac.uk).

Computational Details for TD-DFT Calculations. The model systems used in the theoretical studies of $[Au_2Ag_2(C_6F_5)_4(N{\equiv}CCH_3)_2]_2$ (**1a**) and $[Au_2Ag_2(C_6F_5)_4(N{\equiv}CCH_3)_2]_2$ (**2a**) were taken from the X-ray diffraction data for complexes **1** and **2**, respectively. Keeping all distances, angles, and dihedral angles frozen, single-point DFT calculations were performed on both model systems. In both the ground-state calculations and the subsequent calculations of the electronic excitation spectra, the B3LYP functional[19] as implemented in TURBOMOLE[20] was used. The excitation energies were obtained at the density functional level by using the time-dependent perturbation theory approach (TD-DFT),[21−25] which is a DFT generalization of the Hartree−Fock linear response

Table 3. Selected Bond Lengths [Å] and Angles [deg] for Complex 2[a]

Au−Au#2	2.9129(3)	Au−C(1)	2.043(5)
Au−Cu	2.5876(5)	Au−C(11)	2.090(4)
Au−Cu#1	2.5741(6)	Cu#1−C(11)	2.141(4)
Cu−N	1.903(4)		
C(1)−Au-C(11)	175.92(15)	C(1)−Au−Cu#1	122.71(11)
C(11)−Au−Cu#1	53.43(10)	C(1)−Au−Cu	75.40(11)
C(11)−Au−Cu	103.51(11)	Cu#1−Au−Cu	71.61(2)
C(1)−Au−Au#2	91.18(10)	C(11)−Au−Au#2	92.06(10)
Cu#1−Au−Au#2	141.788(14)	Cu−Au−Au#2	140.501(12)
N−Cu−C(11)#1	128.73(15)	N−Cu−Au#1	121.56(11)
C(11)#1−Cu−Au#1	51.63(11)	N−Cu−Au	103.59(11)
C(11)#1−Cu−Au	127.40(11)	Au#1−Cu−Au	108.39(2)
N−Cu−Cu#1	130.36(11)	C(11)#1−Cu−Cu#1	89.51(11)
Au#1−Cu−Cu#1	54.404(17)	Au−Cu−Cu#1	53.988(16)

[a] Symmetry transformations used to generate equivalent atoms: #1 −*x*+1, −*y*+1, −*z*; #2 −*x*+1, *y*, −*z*+1/2.

Table 4. Spectroscopic and Photophysical Properties of Complexes 1 and 2

complex	medium (*T* [K])	λ_{abs}[nm] (ϵ [mol^{-1} dm^3 cm^{-1}])	λ_{em} (λ_{exc}) [nm]/τ (ns)
1	CH_3CN (298)	211 (6500), 235 (6500), 262 (5100)	nonemissive
	solid (298)	483	547 (510)/231.5, 84.5
	solid (77)		567 (365, 490)
	glass (77)[a]		535, 565 (420, 509)
	CH_3CN (77)		578, 607 (476, 510)
2	CH_2Cl_2 (298)	211 (6500), 235 (6500), 262 (5100)	nonemissive
	solid (298)	493	570 (534)/272.7, 89.1
	solid (77)		594 (364, 519)
	CH_2Cl_2 (77)[a]		514 (350)
	toluene (77)[a]		481 (365)

[a] EtOH/MeOH/CH_2Cl_2 (v/v/v, 8:2:1).

Table 5. TD-DFT Singlet Excitation Calculations for Model $[Au_2Ag_2(C_6H_5)_4(N{\equiv}CCH_3)_2]_2$, 1a

excitation[a]	λ_{calc} (nm)	oscil. str. (s)[b]	contributions[c]
1 (b)	410.0	0.608	142b → 143a (98)
2 (b)	341.8	0.077	140b → 143a (84)
3 (a)	337.0	0.029	140a → 143a (80)
4 (b)	323.4	0.236	139b → 143a (69)
			138b → 143a (21)
5 (b)	311.9	0.097	137b → 143a (82)
6 (b)	307.3	0.120	136b → 143a (86)
7 (a)	306.7	0.014	137a → 143a (87)
8 (b)	291.8	0.028	134b → 143a (47)
			135b → 143a (46)

[a] The symmetry of the excited state is given in parentheses. [b] Oscillator strength shows the mixed representation of both velocity and length representations. [c] Value is |coeff|^2 × 100.

(17) Lide, D. R. In *CRC Handbook of Chemistry and Physics*, 71st ed.; CRC Press: Boston, MA, 1990; p 10.
(18) Sheldrick, G. M. *SHELXL-97*, Program for Crystal Structure Refinement; University of Göttingen: Germany, 1997.
(19) (a) Becke, A. D. *J. Chem. Phys.* **1992**, *96*, 215. (b) Becke, A. D. *J. Chem. Phys.* **1993**, *98*, 5648. (c) Lee, C.; Yang, W.; Parr, R. G. *Phys. Rev. Lett.* **1998**, *B 37*, 785.
(20) Ahlrichs, R.; Bär, M.; Häser, M.; Horn, H.; Kölmel, C. *Chem. Phys. Lett.* **1989**, *162*, 165.
(21) Bauernschmitt, R.; Ahlrichs, R. *Chem. Phys. Lett.* **1996**, *256*, 454.
(22) Bauernschmitt, R.; Ahlrichs, R. *J. Chem. Phys.* **1996**, *104*, 9047.

Table 6. TD-DFT Singlet Excitation Calculations for Model $[Au_2Cu_2(C_6H_5)_4(N{\equiv}CCH_3)_2]_2$, 2a

excitation[a]	λ_{calc} (nm)	oscil. str. (s)[b]	contributions[c]
1 (b)	395.0	0.489	152b → 153a (98)
2 (b)	355.8	0.072	150a → 153a (79)
3 (a)	339.6	0.010	151b → 153a (93)
4 (b)	334.9	0.024	150a → 153a (79)
5 (b)	321.4	0.063	148b → 153a (78)
6 (a)	316.7	0.012	148a → 153a (77)
7 (b)	315.1	0.097	147b → 153a (68)
8 (a)	312.4	0.015	147a → 153a (54)
			146a → 153a (18)
9 (b)	302.1	0.082	142b → 153a (41)
			144b → 153a (22)

[a] The symmetry of the excited state is given in parentheses. [b] Oscillator strength shows the mixed representation of both velocity and length representations. [c] Value is $|\text{coeff}|^2 \times 100$.

(HF-LR) or random-phase approximation (RPA) method.[26] In all calculations, the Karlsruhe split-valence quality basis sets[27] augmented with polarization functions[28] were used (SVP). The Stuttgart effective core potential in TURBOMOLE was used for Au and Ag.[29] Calculations were performed assuming a C_2 symmetry.

Acknowledgment. The D.G.I.(MEC)/FEDER (CTQ2004-05495) project is acknowledged for financial support. M. Monge thanks the MEC-Universidad de La Rioja for his research contract "Ramón y Cajal". M. Montiel thanks the C.A.R. for a grant. Dr. M. A. Laguna is acknowledged for solid-state UV−vis absorption measurements.

Supporting Information Available: X-ray crystallographic data in CIF format for **1** and **2**; figures representing the 3D arrangement of **1** and **2**; phase and modulation curves and normalized residuals of complexes **1** and **2** for lifetime measurements; theoretical excitations for model **2a**; and population analysis for model systems **1a** and **2a**. This material is available free of charge via the Internet at http://pubs.acs.org.

OM060181Z

(23) Bauernschmitt, R.; Häser, M.; Treutler, O.; Ahlrichs, R. *Chem. Phys. Lett.* **1997**, *264*, 573, and references therein.
(24) Gross, E. K. U.; Kohn, W. *Adv. Quantum Chem.* **1990**, *21*, 255.
(25) Casida, M. E. In *Recent Advances in Density Functional Methods, Vol 1*; Chong, D. P., Ed.; World Scientific: Singapore, 1995.
(26) Olsen, J.; Jørgensen, P. In *Modern Electronic Structure Theory, Vol 2*; Yarkony, D. R., Ed.; World Scientific: Singapore, 1995.
(27) Schäfer, A.; Horn, H.; Ahlrichs, R. *J. Chem. Phys.* **1992**, *97*, 2571.
(28) Dunning, T. H., Jr. *J. Chem. Phys.* **1994**, *100*, 5829.
(29) Andrae, D.; Haeussermann, U.; Dolg, M.; Stoll, H.; Preuss, H. *Theor. Chim. Acta* **1990**, *77*, 123.